Cardiovascular Diabetology

RESEARCH

Open Access

Pericoronary adipose tissue radiomics features as imaging markers for coronary artery disease risk assessment: insights from gene expression analysis

Yan Li[1], Weimin Zhang[2], Yahui Hu[3], Zheng Xu[4], Qiang Huo[2], Haicheng Qi[1], Qian Liu[1] and Yan Xing[1,5*]

Abstract

Aims This study aimed to explore the correlation between radiomics features of pericoronary adipose tissue (PCAT) and gene expression in patients with coronary artery disease (CAD), with the goal of identifying novel imaging biomarkers for evaluating CAD.

Methods Between November 2021 and May 2022, data were collected from 60 patients diagnosed with CAD who underwent coronary artery bypass grafting (CABG) and coronary computed tomography angiography (CCTA). Samples of PCAT, three additional adipose tissue types, and peripheral venous blood were analysed. Radiomics features of PCAT were extracted. Gene expression in adipose tissues and serum was quantified via RT-qPCR, immunohistochemistry and ELISA. The correlations between the radiomics features and genes were analysed.

Results Gene expression analysis revealed significantly elevated levels of *CD31*, *MCP-1*, and *leptin* in PCAT compared with other adipose tissues, and the radiomics features of PCAT have a strong correction with the expression of *CD31* and *MCP-1*. At the systemic level, serum analysis revealed increased concentrations of *TNF-α*, *IL-6*, *CD31*, *COL1A1*, and *resistin*, with notable decreases in *ADP* in CAD patients relative to controls. Notably, *CD31*, *ADP*, *IL-6*, and *resistin* were significantly corrlated with PCAT texture features, whereas *TNF-α* was correlated with first-order features.

Conclusions Our findings demonstrated a significant correlation between PCAT radiomics features and gene expression patterns in CAD patients. These features effectively reflect the pathological state of tissues and hold potential as innovative imaging biomarkers. By leveraging PCAT radiomics, clinicians may gain valuable insights for advanced evaluation and management of CAD in later stages.

Keywords Pericoronary adipose tissue, Gene expression, Radiomics, Coronary artery disease

*Correspondence:
Yan Xing
yanxing20@hotmail.com
[1]Imaging Center, The First Affiliated Hospital of Xinjiang Medical University, No 137, LiYuShan South Road, Urumqi 830011, Xinjiang, China
[2]Department of Cardiac Surgery, The First Affiliated Hospital of Xinjiang Medical University, No 137, LiYuShan South Road, Urumqi 830011, Xinjiang, China
[3]School of Basic Medical Sciences, Xinjiang Medical University, Urumqi 830011, Xinjiang, China
[4]Shukun Technology Co., Beijing, China
[5]State Key Laboratory of Pathogenesis, Prevention and Treatment of High Incidence Diseases in Central Asia, Medical Imaging Center, The First Affiliated Hospital of Xinjiang Medical University, Urumqi, Xinjiang, China

Introduction

Coronary artery disease (CAD) is a prevalent cardiovascular condition that consistently maintains the highest mortality rate worldwide [1, 2]. The increasing incidence of CAD poses a serious threat to human life and health. Early diagnosis, treatment and effective preventive measures are very important for reducing CAD mortality [3, 4].

Currently, coronary computed tomography angiography (CCTA) is a widely used noninvasive imaging method for the clinical diagnosis of CAD [5]. Biopsies carry risks of high morbidity and mortality; therefore, identifying gene features through noninvasive imaging can circumvent the need for biopsy while also improving cost-effectiveness [6]. However, replacing biopsies with these imaging techniques in clinical practice necessitates extensive data. Radiomics, an emerging field in medicine, mines and extracts a wealth of quantitative information from medical images to provide valuable support for clinical decision-making [7, 8].

A bidirectional interaction exists between coronary arteries and perivascular adipose tissue [9–11]. PCAT may contribute to the formation of atherosclerosis via paracrine mechanisms and vascular nourishing secretions, ultimately leading to CAD [12, 13]. The expression of *TNF-α*, *MCP-1*, *IL-6*, *COL1A1*, *CD31*, *ADP* (*adiponectin*), *leptin*, and *resistin* in PCAT is closely associated with the development of CAD [14, 15].

Table 1 General clinical data of CAD patients ($\bar{x} \pm s$)

Parameter	Total ($n = 60$)
Age (years)	58.10 ± 0.84
Male (%)	51 (85.0%)
BMI ≥ 30	9 (15.0%)
Risk factor	
Hypertension	30 (50.0%)
Diabetes	18 (30.0%)
Smoking history	25 (41.7%)
Drinking history	17 (28.3%)
Cerebrovascular history	5 (8.3%)
Family history	10 (16.7%)
Drug use	
Aspirin	46 (76.7%)
Clopidogrel hydrochloride	22 (36.7%)
Statins	38 (63.3%)
CABG indications	
Stable angina pectoris	22 (36.7%)
Unstable angina pectoris	31 (51.7%)
Myocardial infarction	7 (11.7%)
TC (mmol/L)	1.75 ± 1.52
TG (mmol/L)	3.71 ± 1.15
LDL (mmol/L)	2.07 ± 0.93
HDL (mmol/L)	0.86 ± 0.25

TC: total cholesterol; TG: triglyceride; LDL: low-density lipoprotein; HDL: high-density lipoprotein

The aim of this study was to investigate the correlation between radiomics features of PCAT and related genes by extracting and screening PCAT radiomics features from CCTA images of CAD patients. Additionally, this study sought to identify the radiomics features that best describe the expression of related genes, and providing new insights into the mechanisms of adverse reactions in coronary artery inflammation and atherosclerosis.

Materials and methods

Study subjects

In this study, CAD patients who underwent coronary artery bypass grafting (CABG)were consecutively enrolled from November 2021 to May 2022. The research was approved by the Ethics Committee of our hospital, and informed consent was obtained from the patients or their families. The inclusion criteria were as follows: ① CAD diagnosis; ② age over 18 years; ③ standardized CCTA examination in accordance with the guidelines for imaging technology use issued by the Cardiothoracic Group of the Imaging Branch of the Chinese Medical Association; and④ CABG performed within one month after CCTA examination. The exclusion criteria were as follows: ① incomplete clinical data; ② cardiac or renal insufficiency; ③ autoimmune diseases; ④ hematological diseases; ⑤ inadequate CCTA image quality according to the diagnostic criteria, as assessed by subjective and objective image quality evaluations; and ⑥ malignant tumor diagnosis.

Prior to initiating cardiopulmonary bypass (CPB), PCAT was obtained from the right coronary artery (adipose tissue in the range of 10–50 mm proximal to the RCA), and adipose tissue surrounding the internal mammary artery (IMA) was taken from the internal thoracic artery (required for heart bypass). Subcutaneous adipose tissue (SAT) was collected from the subcutaneous fat between the skin and the lower end of the sternum, and epicardial adipose tissue (EAT) was acquired from the right heart (right atrium and ventricle). Before surgery, CCTA scans were taken from 60 CAD patients undergoing CABG, from which the radiomic features of PCAT images were extracted. Peripheral venous blood was taken from 60 CAD patients before operation and 60 healthy controls for ELISA. Healthy controls were defined as individuals without clinical signs of CAD, as confirmed by medical history, physical examination, and, when necessary, noninvasive testing. Matching was performed based on age, sex, and body mass index (BMI) to minimize confounding factors that could influence the study's outcome. The clinical data of 60 CAD patients are shown in Table 1. The flow chart of this study is shown in Figs. 1 and 2.

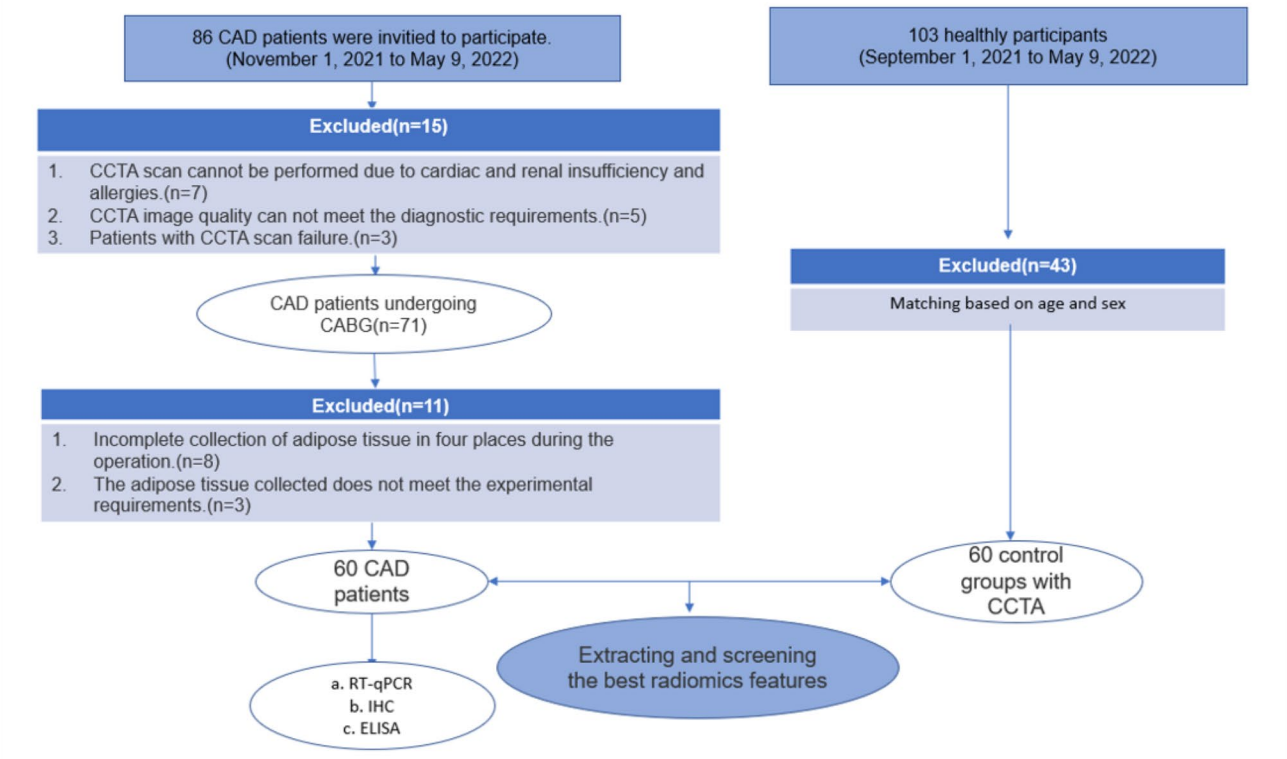

Fig. 1 Flowchart of participant enrolment

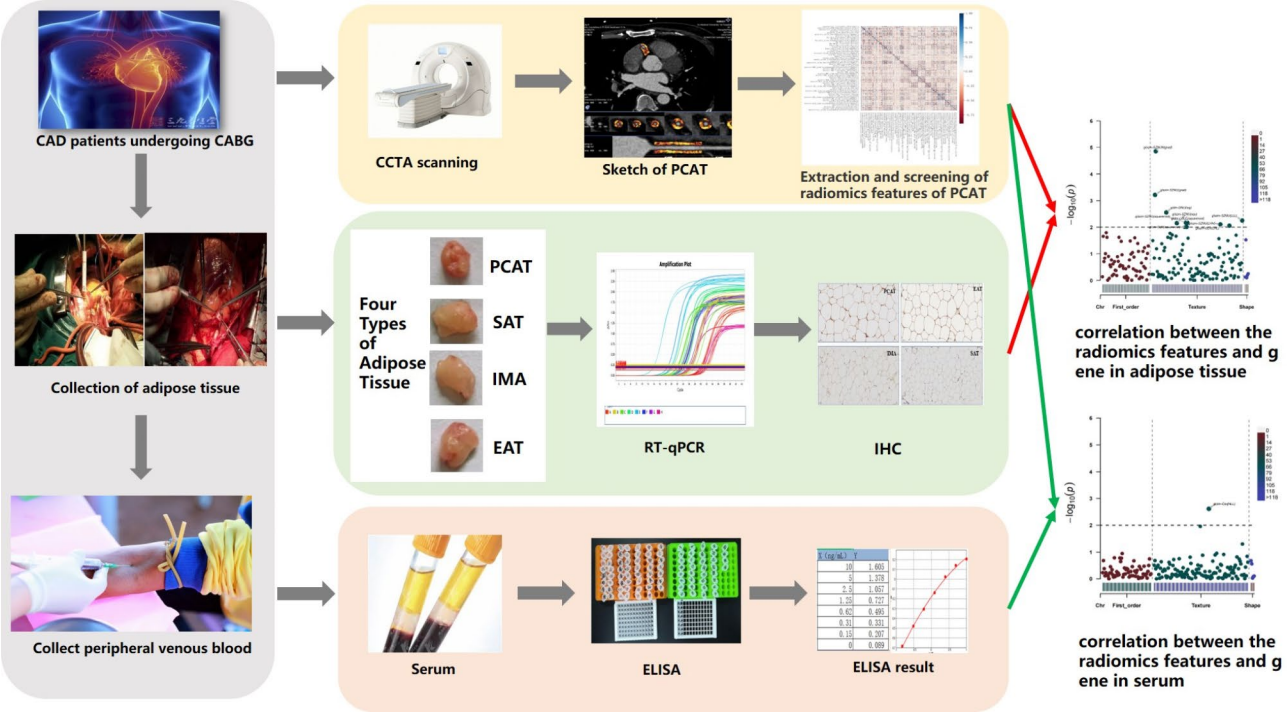

Fig. 2 Research flow chart

CCTA scanning scheme

All CCTA examinations were conducted using 320-row CT devices (Aquilion One Genesis, Canon Medical Systems, Otawara, Japan). The scanning range for CCTA extended from 1.0 cm below the tracheal carina to 1.5 cm below the heart (right ventricle and apex). CCTA scanning uses tracking trigger technology, with the region of interest (ROI) placed at the starting point of the left coronary artery at the aortic root.

A two-phase injection method was applied to administer contrast agent during enhanced scanning [16]. In the first phase, a nonionic contrast agent was infused through the elbow vein at a rate of 3.5–5.0 ml/s, followed by the injection of 30 ml of normal saline at the same speed in the second phase. The CCTA scanning parameters included a tube voltage of 120 kV and a tube current of 380–410 mAs, a detector configuration of 320×0.5 mm, a tube rotation time of 0.28 s, an axial scan range of 0.20–0.35 cm, a scanning plane thickness of 0.5 mm, and a reconstruction interval of 0.25 mm.

Evaluation of CCTA image quality

Objective image quality evaluation: The original transverse image was utilized to assess the completeness of the coronary artery range. Subsequently, the aortic root area at the level of the left coronary artery opening was selected, and the region of interest was set to approximately 1 cm^2; the CT values (HU) and noise were measured within this region.

Subjective image quality evaluation: The 18-segment standard improved segmentation method was implemented to assess the quality of individual images. Employ the Likert 4-level scoring system for coronary artery image quality (with a score of 1 denoting the worst image quality and a score of 4 denoting the best image quality); Blood vessels rated Grade 1 for image quality were considered nonevaluable, whereas those rated Grade 2–4 were defined as evaluable blood vessels. Two physicians, each with 10 years of clinical experience, graded all the images on an image processing workstation (Ziosoft, Tokyo, Japan). The observers were unaware of the reconstruction technology used in the image and the patient's identity.

Extraction and screening of radiomics features via PCAT

In this study, PCAT refers to all voxels with CT values between −190 HU and −30 HU, which corresponded to the diameter of the respective coronary vessels [17]. The 10–50 mm range of the right coronary artery (RCA) was defined as the ROI (the ROI from the image corresponds to the adipose tissue collected during the operation), and PCAT segmentation was automatically performed on the vessel center line using a commercial AI-based image processing tool named 'CoronaryDoc' (Shukun Technology Co., Ltd, Beijing, China), which can distinguish the degree of coronary artery stenosis from the degree of coronary artery lesion. The figure below shows the automatic segmentation of coronary CT images (Fig. 3), which automatically identifies of adipose tissue around the RCA via deep learning and can automatically extract all voxels with CT values of −190 HU ~ −30 HU within 10–50 mm around the corresponding coronary artery.

Radiomics features, including first-order features, a grey level co-occurrence matrix, and shape features of PCAT surrounding the RCA, were extracted via PyRadiomics embedded in the research platform ('UltraScholar', Shukun Technology Co., Ltd, Beijing, China). All the data were randomly divided into a training set (70%) and a test set (30%). The radiomic features of PCAT from CAD patients and healthy individuals were taken as the input, and fivefold cross-validation was used to reduce model overfitting.

The extracted radiomics features were screened to identify the most relevant features for CAD onset. The feature selection process consisted of three steps: (1) preselecting features by excluding those with an absolute Pearson correlation coefficient ≥ 0.9; (2) univariate screening, which relied on univariate feature selection (SelectKBest) to select the best feature through univariate statistical tests; (3) model-based feature selection, which used an absolute shrinkage and selection operator (LASSO) regression model to select the most valuable features within the training set, with a maximum iteration count of 3000, an iteration stopping threshold of 0.0001, and a maximum feature selection count of 200. The selected features were subsequently validated in the testing dataset via three machine learning models. The performance of each model is presented in the supplementary material. Additionally, an external validation dataset, consisting of 72 CAD patients and 72 healthy controls, was collected to further assess the reliability and generalizability of the radiomics models. Detailed results from the external validation analysis are also provided in the supplementary material.

Gene expression analysis

The adipose tissue and serum collected by us were verified via basic experiments to identify the genes most related to CAD. Firstly, RT-qPCR experiments were carried out on four types of adipose tissue. The collected adipose tissue samples were stored at −80℃, RNA was extracted with TRizol (Thermo Fisher), and RNA was transcribed into cDNA via a cDNA reverse transcription kit (TaKara), and gene expression was determined via the Quant Studio TM 6 Real-Time PCR System. The primers used are shown in Table 2. *β-actin* was used as the reference gene, and the relative mRNA expression was

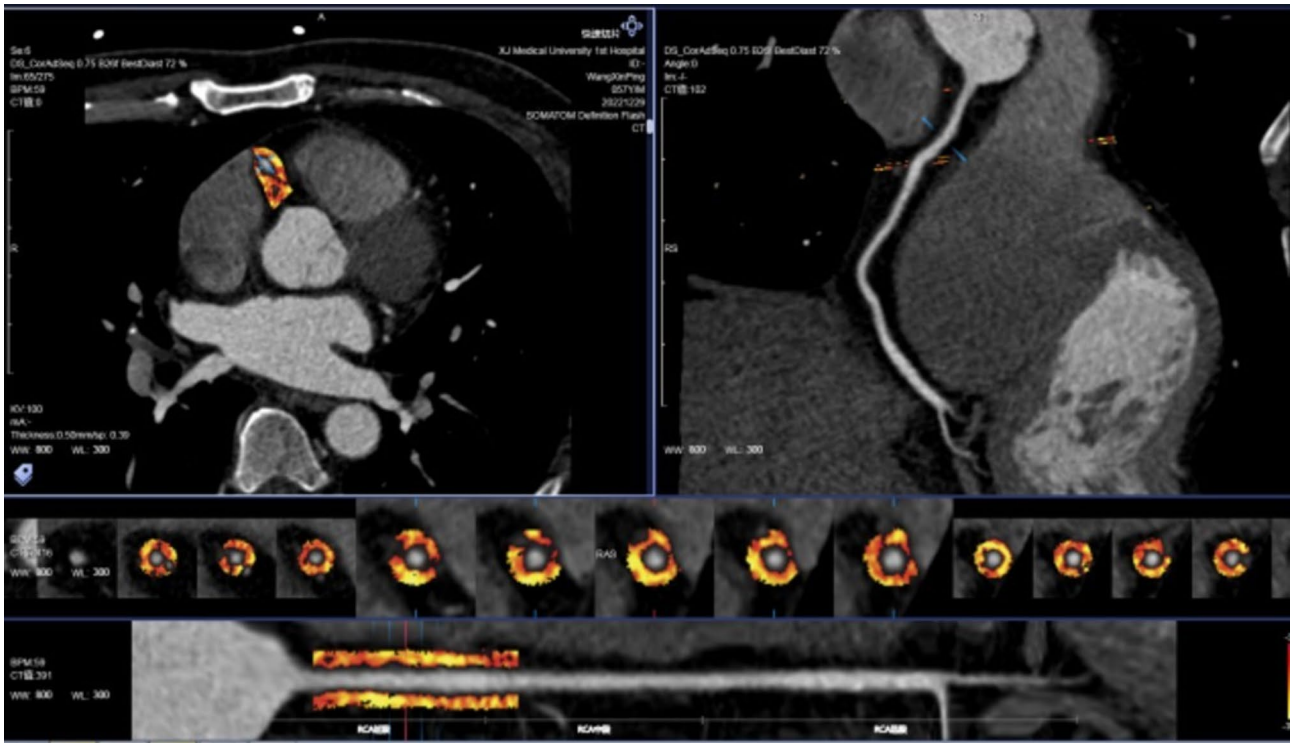

Fig. 3 Automatic drawing of PCAT

Table 2 Primer sequences

Primer name	Primer sequence (5′→3′)
β-actin	F: AGAAAATCTGGCACCACACC R: AATGTGAGCAACGCAGCATAATTCG
Leptin	F: GGCAGGGAAATGGGCAGTGAT G R: AATGTGAGCAACGCAGCATAATTCG
MCP-1	F: GGCTGAGACTAACCCAGAAACATCC R: GGGAATGAAGGTGGCTGCTATGAG
CD31	F: CAAGGTCAGCAGCATCGTGGTC R: TGGGATGGAGCAGGACAGGTTC
IL-6	F: CAAAGAGGCACTGGCAGAAAACAAC R: CCAGGAAAGTCTCCTCATTGAATCC
TNF-α	F: AAGGACACCATGAGCACTGAAAGC R: AGGAAGGAGAAGAGGCTGAGGAAC
ADP	F: ATGGATGAGAGTCCTGGGTGTGAG R: GCAAGGGATTTAGAGGGTGACGGAAG
COL1A1	F: TGATCGTGGTGAGACTGGTCCTG R: CTTTATGCCTCTGTCGCCCTGTTC

determined using the $2^{-\Delta\Delta Ct}$ method [18]. Secondly, the genes screened by RT-qPCR were verified at the protein level (immunohistochemistry). The selected serial sections were subjected to immunohistochemistry via the Universal Elite ABC kit (Vector Laboratories), following the manufacturer's guidelines. The antibodies used for immunohistochemistry were *MCP-1* (ab9858, Abcam, USA; dilution 1:100) and *CD31* (ab182981, Abcam, USA; dilution 1:500), and *leptin* (ab16227, Abcam, USA; dilution 1:200).

Inflammation-related factors(*TNF-α*, *MCP-1*, *ADP*, *leptin*, *IL-6*, and *resistin*), adverse fibrosis(*COL1A1*), and microvascular remodelling (*CD31*) associated with CAD were measured via ELISA kits (Jianglai Biology Science and Technology Co., Ltd.).

Statistical analysis

Clinical data from patients were analysed via SPSS 21.0 software. Our primary objective was to investigate the difference between PCAT and the other three fat depots (EAT, IMA, and SAT) rather than to examine the differences across all four groups simultaneously. For RT-qPCR and ELISA experimental results comparing gene and protein expression levels across the four types of adipose tissue, a paired t-test was used to assess the statistical significance. For continuous variables, means ± SE were used if the data followed a normal distribution. A *p*-value of less than 0.05 was considered statistically significant. GraphPad Prism Version 8.0.1 software was used to create the statistical graphs. The relative gene expression in respective adipose tissue biopsies was summarized using Manhattan plots [-log10(*P*-values) of the Spearman's.rho coefficients].The false discovery rate(FDR) was controlled using the Benjamini-Hochberg [19] procedure. The components accounting for 99.5% of the radiomic variation were first identified. *P*-values from these components were then ranked in ascending order, and significance thresholds were adjusted based on their rank and the

Table 3 Clinical data of CAD patients undergoing CCTA and control group ($\bar{x} \pm s$)

	CAD	Control group	*P*
Total	60	60	
History of hypertension	30(50%)	48(80%)	*P*=0.238
History of diabetes	42(70%)	3(5.0%)	*P*<0.0001*
Smoking history	25(41.67%)	13(21.6%)	*P*<0.0001*
Drinking history	17(28.33%)	19(31.7%)	*P*=0.539
Cerebrovascular history	5(8.33%)	0(0%)	
Family history	10(16.67%)	0(0%)	
BMI (kg/m^2)	25.83±3.75	26.63±4.27	*P*=0.402
TC (mmol/L)	1.75±1.52	1.67±0.81	*P*=0.548
TG (mmol/L)	3.71±1.15	4.31±1.09	*P*<0.0001*
HDL (mmol/L)	0.86±0.25	1.03±0.27	*P*<0.0001*
LDL (mmol/L)	2.07±0.93	2.90±0.89	*P*<0.0001*

total number of tests, with a nominal α=0.05. This procedure ensured a controlled FDR while determining the statistical significance of the results.

Results

Patient characteristics

In this study, PCAT, EAT, and adipose tissue around the IMA and SAT were collected from 60 patients with CAD after excluding 3 patients who failed CCTA scanning, 7 patients who could not undergo CCTA due to allergies and other contraindications, 5 patients whose images did not meet the diagnostic requirements, 8 patients whose adipose tissue collection was incomplete and 3 patients whose samples did not meet the experimental requirements. A comparsion of the clinical data of 60 patients with coronary heart disease and 60 matched controls revealed that the proportion of patients with diabetes, smoking, cerebrovascular history, family history and total cholesterol content in CAD patients were greater among patients with CAD than among healthy controls($P<0.05$). See Table 3 for specific data.

Extraction and screening of Radiomics features of PCAT

From the initial CCTA images, 1688 radiomics features were extracted. Following feature screening, 189 of the original 1688 features were retained based on their significant correlation with CAD incidence. This subset of 189 radiomics features, which consisted of a mixture of 63 first-order features, 5 shape features, and 121 texture features, represents the variables most correlated with CAD incidence. The selected PCAT radiomics features have been verified by the external verification set. This focused approach allowed us to significantly reduce the feature space while preserving the most informative and relevant features for CAD characterization, ensuring that the analysis remained manageable and targeted towards the most predictive indicators of disease onset.

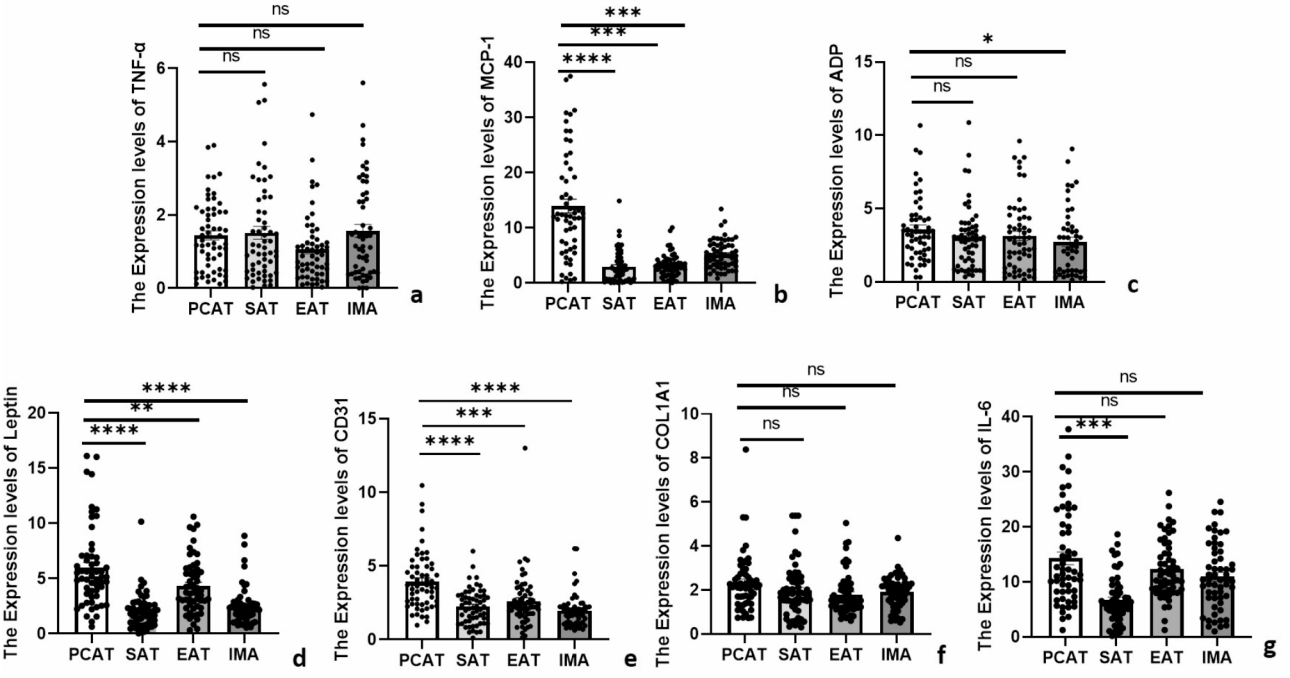

Fig. 4 Statistical chart of the relative expression of genes in adipose tissue at four locations. * means $p<0.05$; ** means $p<0.01$; *** means $p<0.001$; **** means $p<0.0001$

Expression levels of factors related to inflammation, microvascular remodelling and adverse fibrosis in four adipose tissues

PCAT and SAT Comparison: *MCP-1* expression in PCAT (13.94±1.25) significantly differed from that in SAT ($P<0.05$), with a 5.35-fold increase. *Leptin* expression in PCAT (6.01±0.48) was significantly greater than that in SAT ($P<0.05$). *CD31* expression in PCAT (3.94±0.25) was significantly different from that in SAT ($P<0.05$), with a 1.75-fold difference. *IL-6* expression in PCAT was significantly different from that in SAT ($P<0.05$). .

PCAT and EAT Comparison: *MCP-1* expression was significantly higher in PCAT than in EAT ($P<0.05$), with a 3.86-fold difference. *CD31* expression in PCAT and EAT was significantly different(2.61±0.24) ($P<0.05$), with a 1.51-fold difference.

Comparison of PCAT and adipose tissue surrounding the IMA: *MCP-1* expression in PCAT was significantly higher than in adipose tissue surrounding the IMA ($P<0.001$). *Leptin* expression in PCAT was significantly higher than in adipose tissue surrounding the IMA ($P<0.05$), displaying a 2.67-fold difference. *CD31* expression in PCAT significantly differed from adipose tissue surrounding the IMA (1.95±0.15; $P<0.05$), with a 2.02-fold difference(Fig.4).

Immunohistochemical verification of CAD related genes

CD31 is expressed in all four types of adipose tissue (Supplementary Fig. 5), because the fat droplets in adipocytes are relatively large, and positive (brown) cells are distributed around them. Compared with the levels in EAT, SAT and adipose tissue around the IMA, the expression of *CD31* in PCAT was significantly greater ($P<0.05$). *MCP-1* was expressed mainly in the cytoplasm, and the expression of *MCP-1* in PCAT was significantly higher than that in SAT, EAT and adipose tissue around the IMA($P<0.05$). *Leptin* was expressed in the cell membrane and cytoplasm of four adipose tissues, and the expression of *leptin* in PCAT was significantly greater than that in SAT, EAT and adipose tissues around the IMA ($P<0.05$).

The protein levels of molecular markers in the serum detected via ELISA

The *TNF-α* level of CAD patients was 51.03±3.13 ng/ml, which was significantly increased by nearly 3.74 times compared with that of healthy controls ($P<0.05$). The serum *ADP* protein level of patients with CAD was 1999.00±65.84 ng/ml, which was significantly lower than that of healthy controls *(*$P<0.05$). The serum *CD31* concentration in patients with CAD was 25.82±1.23 ng/ml, which was 2.28 times greater than that in the control group (11.35±0.76 ng/ml), The level of *COL1A1* in the serum of patients with CAD was 1.24±0.04 ng/ml, which was significantly greater than that in the control group. The serum *IL-6* concentration of patients with coronary heart disease was 45.22±1.81 ng/ml, and the difference between the two groups was statistically significant ($P<0.05$). *Resistin* in patients with CAD was 5.30 times greater than that in the control group, and the difference was statistically significant ($P<0.05$).

The results demonstrated that the *TNF-α*, *IL-6*, *CD31*, *COL1A1*, and *resistin* in CAD patients were significantly greater than those in the control group ($P<0.05$), whereas the protein levels of *ADP* in CAD patients were significantly lower than those in the control group ($P<0.05$) (Fig. 5).

Correlation analysis of PCAT radiomics features and gene expression

CD31, *MCP-1*, and *leptin* were chosen as target genes for correlation analysis with radiomics features. Based on the correlation analysis between *CD31*, *MCP-1*, and *leptin* with PCAT, the following results were obtained. As depicted in Fig. 6a, *CD31* expression was strongly correlated with 10 texture features among the radiomics features, whereas *leptin* expression was not correlated with the radiomics features. *MCP-1* was sensitive to the first-order features, with its corresponding radiomics feature being lbp-3D-m1_firstorder_10Percentile.

ELISA revealed that the levels of *CD31*, *COL1A1*, *IL-6*, *TNF-α*, and *resistin* in the serum of CAD patients significantly increased, whereas the level of *ADP* significantly decreased. Thus, *CD31*, *COL1A1*, *ADP*, *IL-6*, *TNF-α*, and *resistin* were selected as target genes for correlation analysis with PCAT radiomics. The following results were obtained. As shown in Fig. 7a, among the 121 texture features, *CD31* was highly correlated a high correlation with 10 texture features in the radiomics features, whereas *COL1A1* was not correlated with radiomics features (Fig. 7b). *ADP* was sensitive to four texture features in radiomics, and *IL-6* was significantly correlated with the texture features in radiomics: wavelet_HLL_glcm_Correlation. A clear correlation was observed between *TNF-α* and first-order features in radiomics: wavelet_LLH_First Order_10 Percentile. Among the 121 texture features, *resistin* was more relevant to six texture features in the radiomics, as displayed in Fig. 7f. See Supplementary Tables 3 and Table 4 for the detailed information of the selected histological features.

Discussion

Vascular inflammation and microvascular remodelling are pivotal factors in all stages of atherosclerosis. Structural alterations in adjacent adipose tissue may arise as a consequence of atherosclerosis and vascular inflammation [20]. By analysing radiomics features, we can capture additional information not utilized in current imaging

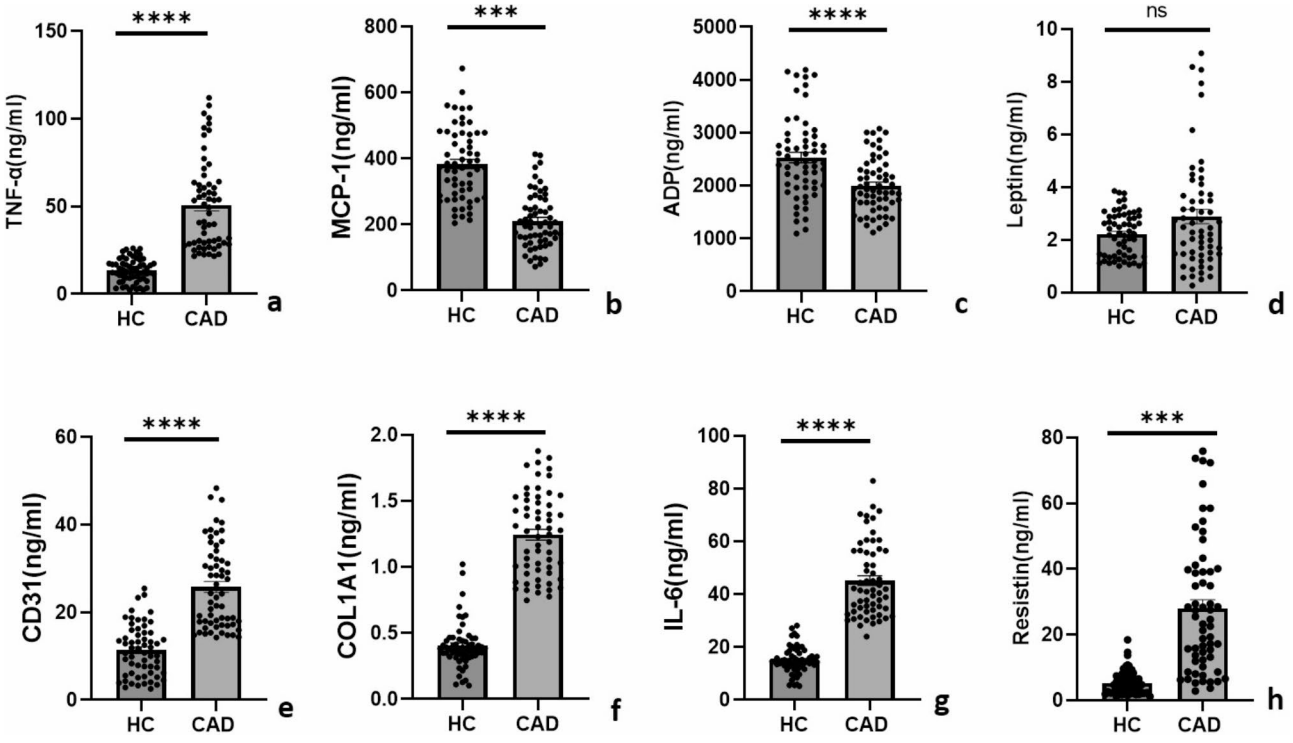

Fig. 5 ELISA results for each gene. * means $p < 0.05$; ** means $p < 0.01$; *** means $p < 0.001$; **** means $p < 0.0001$

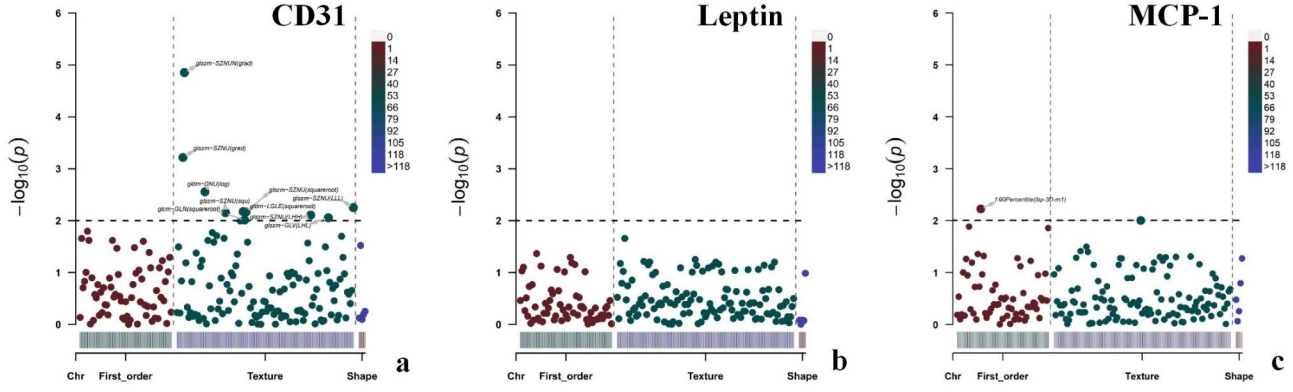

Fig. 6 Manhattan plot of the correlation between the radiomics features of PCAT and the relative expression of each gene in adipose tissue

techniques. More specifically, genomics and proteomics models can be expressed by image-based genomics features derived from macroimages, enabling us to infer disease-related gene information from the quantitative analysis of medical image data, such as CCTA [21].

This study highlights the intricate relationship between radiomics features and gene expression in PCAT and their medical relevance in understanding CAD. Radiomics features, such as texture and first-order features, noninvasively reflect underlying biological processes such as inflammation and microvascular remodelling in PCAT. Specifically, texture features correlate with the expression of *CD31*, which are involved in the structural changes and increased density of PCAT near affected coronary arteries. Meanwhile, first-order features indicate changes in adipocyte characteristics and reflect the impact of inflammatory cytokines, such as *TNF-α* and *MCP-1*, which influence lipid and water contents in adipocytes. Despite the small sample size of patients, who underwent CABG, the difficulty and uniqueness of the four types of adipose tissue acquisition are noteworthy. This dataset provides unique scientific insights, particularly in revealing significant correlations between radiomics features of PCAT and gene expression patterns in CAD, to offer new perspectives into the biological mechanisms of coronary inflammation and atherosclerosis.

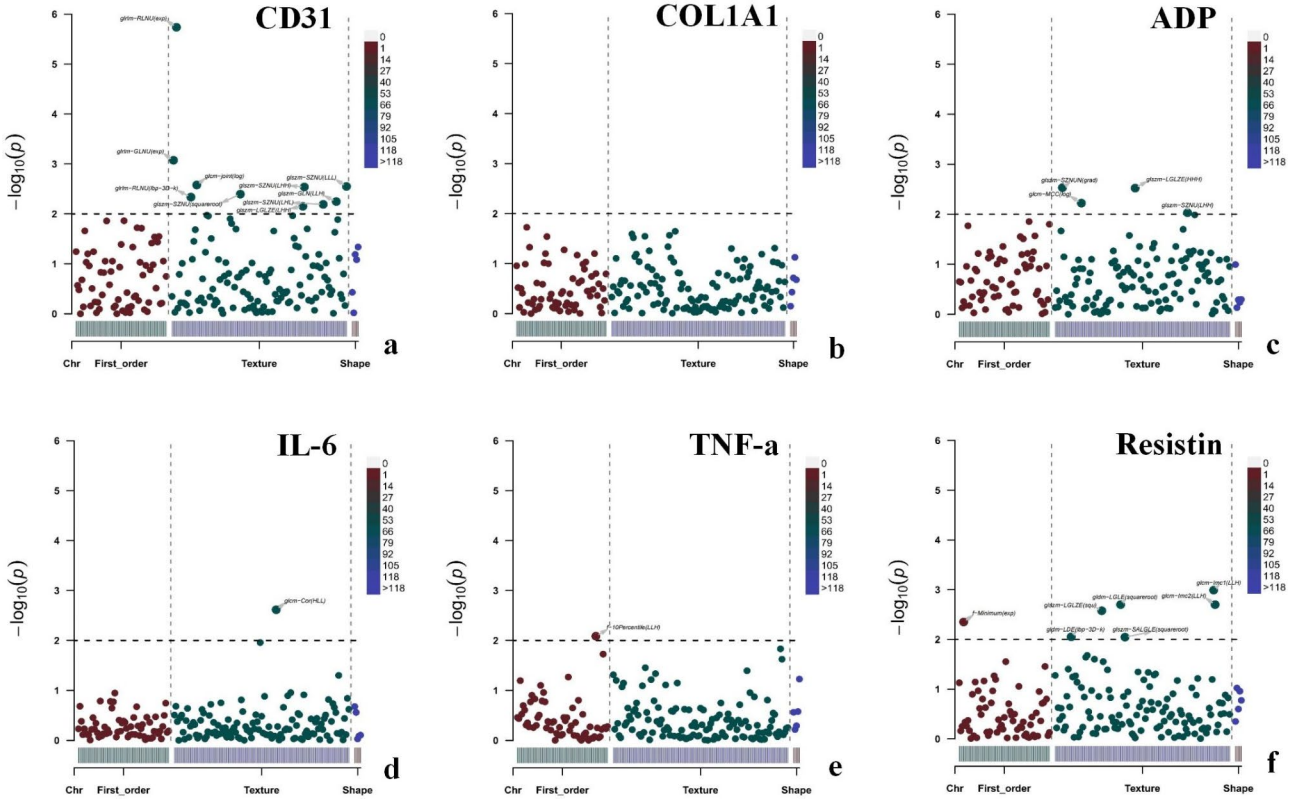

Fig. 7 Manhattan plot showing the correlation between the radiomics features of PCAT and the relative expression of each gene in serum

The role of PCAT in atherosclerosis and the molecular mechanisms involved

The increased expression of *MCP-1* in PCAT suggests that PCAT might play a more substantial role in the initiation and progression of atherosclerosis by enhancing the local inflammatory response [22]. *Leptin*, an adipokine, has been associated with both proinflammatory and proatherogenic effects [23]. The increased expression of *leptin* in PCAT potentially contributes to the development of CAD, possibly through the promotion of inflammation, endothelial dysfunction, or smooth muscle cell proliferation. *CD31*, an endothelial cell marker, has been implicated in angiogenesis and microvascular remodelling [24, 25]. The elevated expression of *CD31* in PCAT suggests that it may contribute to the formation and progression of CAD by promoting neovascularization and microvascular remodelling in the vicinity of the coronary arteries.

Radiomics features and their association with CAD biomarkers in noninvasive detection

Our results suggest that the first-order features of PCAT offer a non-invasive means of detecting *MCP-1* and *TNF-α*, while texture features provide a non-invasive means of detecting *CD31*, *ADP*, *IL-6*, and *resistin*. Research on the relationship between radiomics features and CAD gene expression is limited. In a previous study, a strong correlation was observed between *CD31*, *COL1A1*, and texture features, with first-order features reflecting the presence of *TNF-α* [15]. However, in our study, we found no correlation between serum *COL1A1* and PCAT radiomics features, which may be due to the lack or low expression of *COL1A1* in PCAT in our sample.

Texture features are global features that reflect not only the visual aspects of radiomics images but also the arrangement attributes of objects with gradual or periodic changes in surface structure. Image texture describes the spatial colour distribution and light intensity distribution of an image or a small area within it. Higher texture features indicate uneven spatial colour distribution and light intensity distribution, and local microvascular reconstruction of the coronary artery may cause structural changes in PCAT, leading to an increase in local density and asymmetry compared with unaffected fat [22, 26].

First-order features reflect the symmetry and uniformity of the measured volume pixels and the changes in the local grey distribution of the measured volume pixels, including the median, average, minimum, maximum, standard deviation, and skewness [27]. In the PCAT of CAD patients, a decrease in the adipocyte lipid content, an increase in the water phase reflecting local oedema,

and an increase in the interstitial space become more prominent, leading to voxel changes in adipocytes and other normal cells affected by inflammation in PCAT [28]. Thus, we hypothesize that the enlargement of adipocytes may be associated with the production of proinflammatory factors.

Serum biomarkers and radiomics features in the diagnosis and pathogenesis of CAD

A major innovative aspect of this research is the use of PCAT radiomics features as a noninvasive tool for CAD risk assessment. Notably, we highlight the importance of biopsies in bridging the gap between imaging characteristics and molecular biomarkers, thus offering new insights into the pathophysiological processes of CAD. According to the ELISA results, the levels of secreted *TNF-α*, *IL-6*, *CD31*, *COL1A1* and *resistin* in the serum of CAD patients were significantly greater than those in the serum of healthy controls, whereas the *ADP* level was significantly lower. Previous studies reported that *ADP* can relax blood vessels, prevent atherosclerosis, or directly inhibit the production of inflammatory factors such as *IL-6* and *TNF-α* [29]. The *MCP-1* level in the serum of CAD patients was lower than that in the normal control group. The inflammation of PCAT may not cause an increase in *MCP-1* in the circulatory system, or this effect may have been due accidental factors, such as sample size. In this study, we found that *CD31* and *COL1A1* were significantly increased in CAD patients. Therefore, combined with the above research results, we believe that inflammation, microvascular remodelling and increased serum fibrosis factors are related to the pathogenesis of CAD. At present, serum detection can be considered as the most convenient method to detect molecular markers. In the previous studies, the correlation between imaging and PCAT was analysed at the tissue level, but relevant reports on serology are lacking. This study provides new ideas and methods for the diagnosis of CAD patients by analysing the correlation between serum markers and radiomics features.

Emphasis on the adipose tissue around the RCA

This study focused on the adipose tissue around the RCA because most imaging studies has focused predominantly on the RCA [30]. In CABG, the risk of vascular rupture of adipose tissue around the RCA is lower than that around the left coronary artery [31]. Our results provide valuable insights into the molecular mechanisms involved in the development of CAD by highlighting the distinct gene expression patterns in PCAT compared with those in SAT, EAT, and adipose tissue surrounding the IMA. The significant differences in the expression of *MCP-1*, *leptin* and *CD31* across these adipose tissue types suggest their potential roles in the pathogenesis of CAD.

Advancements in noninvasive CAD risk assessment through radiomics and biomarker correlations

Based on this study, we posit that *MCP-1*, *ADP*, *resistin*, *CD31*, *TNF-α*, and *IL-6* can serve as novel radiologic markers to provide valuable clinical information on the pathogenesis of CAD via noninvasive detection. Moreover, imaging studies in oncology have demonstrated that specific shape and texture-related patterns yield tumour phenotypes that are independently associated with the biological and clinical prognosis of potential tumours [32]. These models typically stem from complex mathematical formulas and are imperceptible to the naked eye by experienced radiologists and clinicians. In a recent study, Kolossvary et al. reported that imaging features can reliably identify HRPs with the napkin ring sign and distinguish metabolic activity from inactive lesions [33]. Through correlation analysis of radiomics features and gene expression, more pathophysiological information of patients can be obtained in a noninvasive manner with the help of image pictures, which is of great significance to the development of clinical work.

Limitations

Presently, this study faces several challenges and limitations. Firstly, as a two-centre study with a relatively small sample size, the findings may not fully represent the broader population. Further multi-center research and in-depth project development are necessary to verify the clinical value of biomarkers based on imageology. Additionally, because it is difficult to collect samples from isolated CAD patients, this study can't rule out the influence of various clinical factors such as gender, abnormal blood sugar, blood pressure and blood lipid, and drug treatment on the research results. Future studies with stratified analysis based on larger datasets could mitigate these issues. Lastly, the gene expression of *resistin* at the adipose tissue level was not verified in this study, warranting further investigation in future research.

Conclusions

In summary, this study highlights the utility of CCTA-based PACT radiomics in capturing molecular and structural changes associated with CAD. Texture features were correlated with inflammatory markers and microvascular remodeling factor, suggesting their involvement in structural modifications and increased tissue density near affected coronary arteries. Meanwhile, first-order features highlighted changes in adipocyte characteristics associated with inflammatory responses, as indicated by alterations in lipid and water contents driven by cytokines, such as *TNF-α* and *MCP-1*. These findings offer valuable insights into the biological changes associated with coronary artery inflammation and atherosclerosis in PCAT. By utilizing these features, we can further

understand the pathogenesis of CAD caused by PCAT, and the radiomics features of PCAT can be used as a non-invasive index to evaluate the occurrence of CAD, which provides the possibility for clinicians to individually evaluate the CAD disease state of patients undergoing CCTA examination in the later stage. The development of PCAT radiomics features provides new methods and opportunities for future CAD evaluation and analysis.

Abbreviations

ADP	Adiponectin
CAD	Coronary artery disease
CABG	Coronary artery bypass grafting
CPB	Cardiopulmonary bypass
CCT	Coronary computed tomography angiography
COL1A1	Collagen type I alpha 1
CD31	Platelet endothelial cell adhesion molecule-1
EAT	Epicardial adipose tissue
IMA	Internal mammary artery
LASSO	Least absolute shrinkage and selection operator
MCP-1	Monocyte chemoattractant protein-1
PCAT	Pericoronary adipose tissue
ROI	Region of interest
RCA	Right coronary artery
RT-qPCR	Quantitative real-time PCR
SAT	Subcutaneous adipose tissue
VOI	Volume of interest
IMA	Internal mammary artery

Supplementary Information

The online version contains supplementary material available at https://doi.org/10.1186/s12933-024-02530-6.

Supplementary Material 1

Acknowledgements

We are very grateful to Yue Wu from the Imaging Center of People's Hospital of Xinjiang Uygur Autonomous Region for providing us with external verification data, and we thank Zicheng Zhao from Canon Medical Systems for technical support.

Author contributions

LY, XZ and XY designed and conducted this research. HYH and QHC were responsible for data collection. LY，ZWM, LQ and HQ analyzed the data, and drafted and revised the manuscript. All the authors read and approved the final version of the manuscript.All authors reviewed the manuscript.

Funding

This study was supported by the National Natural Science Foundation of China(Grant No.82160334), State Key Laboratory of Pathogenesis,Prevention and Treatment of High Incidence Diseases in Central Asia Fund(SKL-HIDCA-2023-10) and the National Natural Science Foundation of China (Grant No. 82460346).

.

Availability of data and materials

No datasets were generated or analysed during the current study.

Declarations

Ethics approval and consent to participate

This research was approved by the First Affiliated Hospital of Xinjiang Medical University. All methods were carried out in accordance with relevant guidelines and regulations. All the subjects have provided informed consent to participate in this study.

Competing interests

The authors declare no competing interests.

Received: 23 August 2024 / Accepted: 27 November 2024
Published online: 18 December 2024

References

1. Leong DP, Joseph PG, McKee M, et al. Reducing the global burden of cardiovascular disease, part 2: prevention and treatment of cardiovascular disease. Circ Res. 2017;121(6):695–710.
2. Urban P, Mehran R, Colleran R, et al. Defining high bleeding risk in patients undergoing percutaneous coronary intervention: a consensus document from the Academic Research Consortium for high bleeding Risk. Eur Heart J. 2019;40(31):2632–53.
3. Shaya GE, Leucker TM, Jones SR, Martin SS, Toth PP. Coronary heart disease risk: low-density lipoprotein and beyond. Trends Cardiovasc Med. 2022;32(4):181–94.
4. Narula N, Olin JW, Narula N. Pathologic disparities between peripheral artery disease and coronary artery disease. Arterioscler Thromb Vasc Biol. 2020;40(9):1982–9.
5. Cury RC, Leipsic J, Abbara S, et al. CAD-RADS™ 2.0–2022 coronary artery disease-reporting and data system: an expert consensus document of the Society of Cardiovascular Computed Tomography (SCCT), the American College of Cardiology (ACC), the American College of Radiology (ACR), and the North America Society of Cardiovascular Imaging (NASCI). J Cardiovasc Comput Tomogr. 2022;16(6):536–57.
6. Hartmann K, Sadée CY, Satwah I, et al. Imaging genomics: data fusion in uncovering disease heritability. Trends Mol Med. 2023;29(2):141–51.
7. Avanzo M, Wei L, Stancanello J, et al. Machine and deep learning methods for radiomics. Med Phys. 2020;47(5):e185-202.
8. Chan RC, To CKC, Cheng KCT, Yoshikazu T, Yan LLA, Tse GM. Artificial intelligence in breast cancer histopathology. Histopathology. 2023;82(1):198–210.
9. Mikołajczyk TP, Guzik TJ. Perivascular adipose tissue as the secret behind resistance to atherosclerosis exhibited by the human internal mammary artery. Kardiol Pol. 2020;78(12):1194–6.
10. Hu H, Garcia-Barrio M, Jiang ZS, et al. Roles of perivascular adipose tissue in hypertension and atherosclerosis. Antioxid Redox Signal. 2021;34(9):736–49.
11. Mancio J, Oikonomou EK, Antoniades C. Perivascular adipose tissue and coronary atherosclerosis. Heart. 2018;104(20):1654–62.
12. Chen JY, Wu YP, Li CY, et al. PPARγ activation improves the microenvironment of perivascular adipose tissue and attenuates aortic stiffening in obesity. J Biomed Sci. 2021;28(1):22.
13. Evangelos K, Oikonomou. The role of adipose tissue in cardiovascular health and disease. Nat Rev Cardiol. 2019;16(2):83–99.
14. Dugani SB, Moorthy MV, Li C, et al. Association of lipid, inflammatory, and metabolic biomarkers with age at onset for incident coronary heart disease in women. JAMA Cardiol. 2021;6(4):437–47.
15. Oikonomou EK, Williams MC, Kotanidis CP, et al. A novel machine learning-derived radiotranscriptomic signature of perivascular fat improves cardiac risk prediction using coronary CT angiography. Eur Heart J. 2019;40(43):3529–43.
16. Liu JB, Zhang JW, Zhang XH, Zhou W, Yuan B, Fan LJ. Feasibility study of contrast injection scheme based on body mass and iodine flow rate in coronary computed tomography angiography with wide detector CT. Zhonghua Yi Xue Za Zhi. 2020;100(43):3448–52.
17. Kotanidis CP, Antoniades C. Perivascular fat imaging by computed tomography (CT): a virtual guide. Br J Pharmacol. 2021;178(21):4270–90.
18. Li S, Yang M, Zhao Y, et al. Deletion of ASPP1 in myofibroblasts alleviates myocardial fibrosis by reducing p53 degradation. Nat Commun. 2024;15(1):8425.
19. Yoav B, Yosef H. Controlling the false discovery rate: a practical and powerful approach to multiple testing. J R Stat Soc Ser B (Methodol.).1995;289–300.
20. Tan N, Dey D, Marwick TH, Nerlekar N. Pericoronary adipose tissue as a marker of cardiovascular risk: JACC review topic of the week. J Am Coll Cardiol. 2023;81(9):913–23.
21. Hobbs SK, Shi G, Homer R, et al. Magnetic resonance image-guided proteomics of human glioblastoma multiforme. J Magn Reson Imaging. 2003;18(5):530–6.
22. Chatterjee TK, Aronow BJ, Tong WS, et al. Human coronary artery perivascular adipocytes overexpress genes responsible for regulating vascular morphology, inflammation, and hemostasis. Physiol Genomics. 2013;45(16):697–709.

23. Landecho MF, Tuero C, Valentí V, et al. Relevance of leptin and other adipokines in obesity-associated cardiovascular risk. Nutrients. 2019;11(11):2664.
24. Caligiuri G. Mechanotransduction, immunoregulation, and metabolic functions of CD31 in cardiovascular pathophysiology. Cardiovasc Res. 2019;115(9):1425–34.
25. Caligiuri G. CD31 as a therapeutic target in Atherosclerosis. Circ Res. 2020;126(9):1178–89.
26. van Timmeren JE, Cester D, Tanadini-Lang S, Alkadhi H, Baessler B. Radiomics in medical imaging-how-to guide and critical reflection. Insights Imaging. 2020;11(1):91.
27. Lambin P, Rios-Velazquez E, Leijenaar R, et al. Radiomics: extracting more information from medical images using advanced feature analysis. Eur J Cancer. 2012;48(4):441–6.
28. Kern PA, Ranganathan S, Li C, et al. Adipose tissue tumor necrosis factor and interleukin-6 expression in human obesity and insulin resistance. Am J Physiol Endocrinol Metab. 2001;80(5):E745–51.
29. Choi HM, Doss HM, Kim KS. Multifaceted physiological roles of adiponectin in inflammation and Diseases. Int J Mol Sci. 2020;21(4):1219.
30. Goeller M, Tamarappoo BK, Kwan AC, et al. Relationship between changes in pericoronary adipose tissue attenuation and coronary plaque burden quantified from coronary computed tomography angiography. Eur Heart J Cardiovasc Imaging. 2019;20(6):636–43.
31. Antonopoulos AS, Sagris M, Tousoulis D. Reply to: assessment of pericoronary adipose tissue attenuation. Eur Heart J Cardiovasc Imaging. 2023;24(4):e58.
32. Aerts HJ, Velazquez ER, Leijenaar RT, et al. Decoding tumour phenotype by noninvasive imaging using a quantitative radiomics approach. Nat Commun. 2014;5:4006.
33. Kolossváry M, Karády J, Szilveszter B, et al. Radiomic features are superior to conventional quantitative computed tomographic metrics to identify coronary plaques with napkin-ring sign. Circ Cardiovasc Imaging. 2017;10(12):e006843.

Publisher's note